Ukrainian Journal of Physical Optics
ISSUE 2
2026

EXTREME VALUES OF PHOTOELASTIC EFFECTS IN BTAS AND BTGS CRYSTALS

N. DEMYANYSHYN [1], B. MYTSYK [1], O. LISHCHUK [2], P. SOLOMENCHUK [2], A. ANDRUSHCHAK [2]

[1] Karpenko Physico-Mechanical Institute, 5 Naukova Str., 79601, Lviv, Ukraine
[2] Lviv Polytechnic National University, 12 Bandery Str., 79046, Lviv, Ukraine

Received: 05.05.2026

Abstract. Indicative surfaces (ISs) of the spatial distribution of piezo-optic and elasto-optic effects (POE and ELOE) in $Ba_3TaAl_3Si_2O_{14}$ (BTAS) and $Ba_3TaGa_3Si_2O_{14}$ (BTGS) langasite-type crystals were constructed based on piezo-optic π_{im} and elasto-optic p_{in} coefficient matrices obtained from first-principles calculations. We presented relations for the ISs of longitudinal and transverse POE and ELOE, as well as relations for the ELOE induced by shear strains. It is shown that the POE and ELOE properties of BTAS and BTGS crystals are essentially anisotropic, while the largest values of the transverse ELOE of BTAS and BTGS crystals (0.213 and 0.209, respectively) do not coincide with the directions of the crystallophysical axes of these crystals. According to these ELOE values, these crystals exceed other langasite-group crystals, $La_3Ga_5SiO_{14}$ (LGS) and $Ca_3TaGa_3Si_2O_{14}$ (CTGS), by a factor of 2-3. For all the above crystals, ELOE surfaces induced by shear strains have been constructed. The maximum values of these surfaces (0.108-0.131) are nearly two times lower than the maxima of the transverse ELOE in BTAS and BTGS crystals, but the acousto-optic efficiency can be relatively high due to the low acoustic-wave velocities caused by shear strains.

Keywords: photoelasticity, quantum-mechanical calculation, langasite-group crystals, indicative surfaces
UDC: 535.551
DOI: 10.3116/16091833/Ukr.J.Phys.Opt.2026.02157

1. Introduction

With advances in computer technology, it has become possible to predict the physical properties of materials using first-principles calculations [1-4]. There are many works, for example [5-8], on the successful application of this approach to studying and predicting material properties. Since photoelastic interferometric studies are complex and labor-intensive [9, 10], first-principles predictions should be used as an effective tool for the preliminary evaluation of materials suitable for application in photoelastic and acousto-optic light-modulation devices.

Optically uniaxial crystals of the langasite group possess a unique combination of different physical properties. For example, they are characterized by low acoustic-wave attenuation (several times lower than in quartz [11]), temperature stability of physical characteristics, in particular elastic characteristics [12], a high optical-damage threshold [13, 14], as well as large piezoelectric effect and electromechanical coupling coefficient [15]. Langasite $La_3Ga_5SiO_{14}$ (LGS) is the best-known gallosilicate. However, the efforts of researchers aimed at improving material quality and optimizing growth technology have led to the creation of a group of compounds (about 100 crystals [16, 17], the list of which is constantly expanding) that are structurally close to langasite. Such crystals are already widely used in the manufacture of pressure and detonation sensors, substrates for thermally stable cuts for acoustoelectronic filters based on surface and bulk acoustic waves, Q-switches, and temperature-stable broad-

band monolithic filters used in mobile communication systems (see, for example, [18-21]). However, the photoelastic properties (piezo- and elasto-optic effects) of LGS-group crystals have been experimentally studied only for a few representatives, LGS and CTGS [22-24].

Since crystalline materials possess substantially anisotropic photoelastic properties, it is important not only to determine the magnitudes of the piezo- or elasto-optic coefficients (POCs or ELOCs) of such materials but also to study the spatial distribution of photoelastic effects in them in order to evaluate the efficiency of their application, for example, in optical-radiation modulators. For such an analysis, methods for optimizing piezo-, elasto-, and acousto-optic interaction in crystalline materials are widely used [25-32].

In this work, the spatial anisotropy of photoelastic effects in $Ba_3TaAl_3Si_2O_{14}$ (BTAS) and $Ba_3TaGa_3Si_2O_{14}$ (BTGS) crystals, belonging to the langasite group [8, 33], is analyzed based on POCs and ELOCs calculated using a quantum-mechanical method. The obtained results are compared with the results for other crystals of this group: $La_3Ga_5SiO_{14}$ (LGS) and $Ca_3TaGa_3Si_2O_{14}$ (CTGS) [25].

2. Characteristics of the objects of study

Crystals of the langasite group belong to symmetry class 32 (space group P321) [16, 17]. Despite the small number (eight) of independent components of the matrices of piezo-optic and elasto-optic effects (POE and ELOE), these matrices for LGS and CTGS crystals have been filled by interferometric and polarization-optical methods relatively recently [22-24]. Since experimental methods are labor-intensive, the photoelastic properties of some langasite-group crystals (CTGS, CNGS, and BTGS) have been calculated by a quantum-mechanical method [31, 34]. The calculated POC values, for example, for CTGS, are in good agreement with the experimentally determined coefficients [31]. In particular, the deviations from the arithmetic mean values between the calculated and experimental POCs do not exceed ±15% for π_{13} and π_{31} and ±5% for the coefficients π_{33}, π_{41}, π_{14}, and π_{44}.

In this work, the calculation of the POCs, ELOCs, and elastic stiffness and compliance coefficients was performed for BTAS crystals in order to study the influence on the photoelastic properties of replacing the expensive gallium (Ga) element in the crystal structure with the cheaper aluminum (Al) element. The calculation was carried out using the Crystal17 program, following the approach used in [31, 34]. These works substantiate the use of the PBE0 hybrid functional, as well as other parameters employed in the calculations of the POC π_{im} and ELOC p_{ik}. The specified hybrid functional also provides good agreement between the calculated and experimental values of π_{im} and p_{ik} in tetragonal $CaWO_4$ [35] and $PbMoO_4$ [36] crystals. The methodology for calculating piezo- and elasto-optic coefficients in crystals is described in detail in [35, 37]. The BTAS lattice parameters indicated in [8, 38] were used for the calculation: a = 8.456 і c = 5.121 Å.

The results of calculating all independent POCs π_{im} and ELOCs p_{ik} of BTAS crystals are given in Table 1. For comparison, this table also includes the POCs and ELOCs of BTGS, LGS, and CTGS crystals. In addition, Table 1 presents the calculated values of the elastic stiffness C_{mk} and elastic compliance S_{km} coefficients for BTAS crystals, which can be used to verify the consistency of the piezo-optic and elasto-optic coefficients on the basis of the well-known tensor relations $\pi_{im}=p_{ik}S_{km}$ and $p_{ik} = \pi_{im}C_{mk}$ [39, 40].

As shown in the table, the largest POC values for BTAS crystals were smaller than the corresponding POC values for BTGS crystals. BTGS crystals have two large principal POCs,

Table 1. Elastic C_{mk} and S_{km}, piezo-optic π_{im}, and elasto-optic p_{ik} coefficients of LGS and CTGS crystals (experimental data) and BTGS and BTAS crystals (calculated by a quantum-mechanical method).

C_{mk}, 10^9 N/m^2	C_{11}	C_{12}	C_{13}	C_{31}	C_{33}	C_{14}	C_{41}	C_{44}
BTAS	175.3	74.6	84.8	84.8	197.9	–7.1	–7.1	72.3
S_{km}, 10^{-12} m^2/N	S_{11}	S_{12}	S_{13}	S_{31}	S_{33}	S_{14}	S_{41}	S_{44}
BTAS	7.86	2.21	2.42	2.42	7.13	0.99	0.99	14.03
π_{im}, Br	π_{11}	π_{12}	π_{13}	π_{31}	π_{33}	π_{14}	π_{41}	π_{44}
LGS [22]	–0.17 ±0.06	0.10 ±0.07	0.30 ±0.07	0.70 ±0.19	–1.25 ±0.08	0.32 ±0.15	0.33 ±0.12	0.35 ±0.16
CTGS [24]	–0.19 ±0.06	0.22 ±0.09	0.53 ±0.12	1.40 ±0.19	–1.20 ±0.09	0.72 ±0.11	0.32 ±0.11	–0.81 ± 0.40
BTGS [34]	–0.18	0.65	0.78	**1.31**	**–1.48**	0.26	0.11	–0.46
BTAS	0.06	0.57	0.75	1.14	–1.09	0.25	0.18	–0.21
p_{ik}	p_{11}	p_{12}	p_{13}	p_{31}	p_{33}	p_{14}	p_{41}	p_{44}
LGS [24]	0.014* ±0.016	0.027 ±0.017	0.071 ±0.021	0.078 ±0.047	–0.181 ±0.049	0.013 ±0.009	0.033 ±0.027	0.028 ±0.009
CTGS [24]	0.008* ±0.010	0.044 ±0.013	0.096 ±0.022	0.165 ±0.031	–0.088 ±0.031	0.029 ±0.005	0.029 ±0.015	–0.033 ±0.017
BTGS [34]	0.080	0.162	0.189	0.185	–0.067	0.023	0.013	–0.032
BTAS	0.115	0.170	**0.202**	**0.193**	–0.022	0.022	0.019	–0.019

*The values of the p_{11} coefficient for LGS and CTGS are smaller than the errors of their determination.

π_{31} and π_{33}, and the coefficient π_{33} = –1.48 Br is the largest among the POCs presented in Table 1. Other large POCs π_{13} of BTAS and BTGS crystals, exceed the corresponding POCs of LGS and CTGS crystals by approximately ~ 1.5–2.5.

Regarding the ELOCs, BTAS crystals exhibit the largest values (p_{31} = 0.202 and p_{33} = 0.193). That is, the replacement of the Ga^{3+} gallium cation in the BTGS structure by the Al^{3+} aluminum cation results in an improvement of the elasto-optic properties of the BTAS structure. In addition, the largest ELOCs p_{13} and p_{31} of BTAS and BTGS crystals exceed the largest ELOC p_{33} of langasite, while the ELOC p_{12} of BTAS and BTGS is 4-5 times larger than in LGS and CTGS crystals. Therefore, it is expedient to construct surfaces of the spatial distribution of POE and ELOE and to find the maximum values of these effects and their directions relative to the crystallophysical axes.

3. Analytical relations for indicative surfaces of POE and ELOE

For a study of the anisotropy of POE and ELOE, a geometrical representation of higher-rank tensors, namely indicative surfaces (ISs), is used [25, 30]. Mathematically, the IS formula corresponds to the law of transformation of tensor components when passing from one coordinate system to another. For the IS of POE (a fourth-rank tensor), this expression is presented as

$$\pi'_{ijkl} = \alpha_{im}\alpha_{jn}\alpha_{kp}\alpha_{lo}\pi_{mnpo}. \quad (1)$$

Let's mention that, when constructing ISs on the basis of (1), the nonzero POCs π_{mnpo} corresponding to the POE matrix of a crystal of a particular symmetry class are taken into account, and the corresponding direction cosines α_{im}, α_{jn}, α_{kp}, α_{lo} of the radius vector $\boldsymbol{R}$ describing the IS are written in the spherical coordinate system θ, φ as [25, 30]:

$$\alpha_{r1} = \sin\theta\cos\varphi, \quad \alpha_{r2} = \sin\theta\sin\varphi, \quad \alpha_{r3} = \cos\theta. \tag{2}$$

From Eqs. (1) and (2), taking into account the nonzero components of the POC matrix for crystals belonging to the point group of symmetry 32, one obtains the known expression [25] for the IS whose radius vector describes the POE π'_{im} in arbitrary directions ***i*** of light polarization under the action of uniaxial pressure in any specified direction ***m***:

$$\begin{aligned}\pi'_{im} = {} & [\pi_{11}\sin^2\theta_m\cos^2(\varphi_m-\varphi_i) + \pi_{12}\sin^2\theta_m\sin^2(\varphi_m-\varphi_i) + \pi_{13}\cos^2\theta_m \\ & +0.5\pi_{14}\sin 2\theta_m\sin(\varphi_m+2\varphi_i)]\sin^2\theta_i + (\pi_{31}\sin^2\theta_m + \pi_{33}\cos^2\theta_m)\cos^2\theta_i \\ & +[\pi_{41}\sin^2\theta_m\sin(2\varphi_m-\varphi_i) + 0.5\pi_{44}\sin 2\theta_m\cos(\varphi_m-\varphi_i)]\sin 2\theta_i.\end{aligned} \tag{3}$$

where π_{im} – are POCs expressed in two-index (matrix) notation [39, 40]; θ_i, φ_i, θ_m, φ_m are the spherical coordinates for the directions of polarization of the light wave ***i*** and action of uniaxial pressure ***m***, respectively.

For the longitudinal POE, when vectors ***i*** and ***m*** coincide (***i*** $||$ ***m***) and, accordingly, $\theta = \theta_m = \theta_i$, $\varphi = \varphi_m = \varphi_i$, the IS formula is following:

$$\begin{aligned}\pi'_{ii}(\theta,\varphi) = \pi'_{ii} = {} & \pi_{11}\sin^4\theta + \pi_{33}\cos^4\theta + (\pi_{13}+\pi_{31}+2\pi_{44})\sin^2\theta\cos^2\theta \\ & +(\pi_{14}+2\pi_{41})\sin^3\theta\cos\theta\sin 3\varphi.\end{aligned} \tag{4}$$

For the transverse POE (**i**$\perp$**m**), two construction variants are possible: 1) the spherical coordinates specifying the directions of vectors i and m are related by $\theta_m = 90°$, $\varphi_m = \varphi_i + 90°$, 2) $\theta_i = 90°$, $\varphi_i = \varphi_m + 90°$. As a result, one obtains the IS of light polarization $\pi'^{(i)}_{im}$ (constructed by the radius vector that coincides with the polarization direction of the electromagnetic wave **i**) and the IS of mechanical stress $\pi'^{(m)}_{im}$ (constructed by the radius vector that coincides with the direction **m** of uniaxial pressure), respectively:

$$\pi'^{(i)}_{im} = \pi_{12}\sin^2\theta_i + \pi_{31}\cos^2\theta_i - 2\pi_{41}\sin\theta_i\cos\theta_i\sin 3\varphi_i, \tag{5}$$

$$\pi'^{(m)}_{im} = \pi_{12}\sin^2\theta_m + \pi_{13}\cos^2\theta_m - \pi_{14}\sin\theta_m\cos\theta_m\sin 3\varphi_m. \tag{6}$$

The analog of Eq. (3) for the ELOE is the expression [25]

$$\begin{aligned}p'_{ik} = {} & [p_{11}\sin^2\theta_k\cos^2(\varphi_k-\varphi_i) + p_{12}\sin^2\theta_k\sin^2(\varphi_k-\varphi_i) + p_{13}\cos^2\theta_k \\ & +p_{14}\sin 2\theta_k\sin(\varphi_k+\varphi_i)]\sin^2\theta_i + (p_{31}\sin^2\theta_k + p_{33}\cos^2\theta_k)\cos^2\theta_i \\ & +[p_{41}\sin^2\theta_k\sin(2\varphi_k+\varphi_i) + p_{44}\sin 2\theta_k\cos(\varphi_k-\varphi_i)]\sin 2\theta_i,\end{aligned} \tag{7}$$

where the index k denotes the direction of strain in the crystal, and p_{ik}. are the elasto-optic coefficients.

Based on (7), it is easy to write analogs of expressions (4)-(6), which describe the longitudinal (**i** $||$ **k**) and two transverse (**i**$\perp$**k**) ELOEs; they are not presented here because of their similarity to the indicated piezo-optic analogs.

Let's also use the expression for the IS of the ELOE under the action of shear strains in planes that include the X_3 axis [25]:

$$\begin{aligned}p'_{ik} = p'(\theta_i,\varphi_i,\theta_k,\varphi_k) = {} & 0.5(p_{11}\cos^2\varphi_k + p_{12}\sin^2\varphi_k - p_{13})\sin^2\theta_i\cos^2\varphi_i\sin 2\theta_k \\ & +0.5(p_{12}\cos^2\varphi_k + p_{11}\sin^2\varphi_k - p_{13})\sin^2\theta_i\sin^2\varphi_i\sin 2\theta_k \\ & +0.5(p_{31}-p_{33})\cos^2\theta_i\sin 2\theta_k + p_{14}\sin^2\theta_i\cos 2\theta_k\sin(\varphi_k+2\varphi_i) \\ & +0.5p_{41}\sin 2\theta_i\sin 2\theta_k\sin(2\varphi_k+\varphi_i) + p_{44}\sin 2\theta_i\cos 2\theta_k\cos(\varphi_i-\varphi_k) \\ & +0.25(p_{11}-p_{12})\sin^2\theta_i\sin 2\varphi_i\sin 2\theta_k\sin 2\varphi_k.\end{aligned} \tag{8}$$

and, based on this expression, write formulas for two particular cases:

1) The formula for the ELOE IS for shear strains in the X_1X_3 plane under the conditions $\theta_k = 0°$, $\varphi_k = 0°$:

$$p'_{ik} = p'(\theta_i,\varphi_i,0°,0°) = p_{14}\sin^2\theta_i \sin 2\varphi_i + p_{44}\sin 2\theta_i \cos\varphi_i\,; \tag{9}$$

2) The formula for the ELOE IS for shear strains in the X_1X_3 plane under the conditions $\theta_k = 45°$, $\varphi_k = 0°$:

$$\begin{aligned} p'_{ik} = p'(\theta_i,\varphi_i,45°,0°) = {} & 0.5(p_{11}\sin^2\varphi_i + p_{12}\cos^2\varphi_i)\sin^2\theta_i - 0.5p_{13}\sin^2\theta_i \\ & + 0.5(p_{31} - p_{33})\cos^2\theta_i + 0.5p_{41}\sin 2\theta_i \sin\varphi_i. \end{aligned} \tag{10}$$

4. Results and discussion

Examples of ISs and their sections by the X_2X_3 plane for the longitudinal and transverse POE and ELOE of BTAS and BTGS crystals, constructed on the basis of Eqs. (4)-(6) and the values of POCs π_{im} and ELOCs p_{ik}, taken from Table 1, are presented in Fig. 1. Tables 2 and 3 give the largest values of POE and ELOE of these crystals and the corresponding geometries of piezo- and elasto-optic interaction.

The ISs of longitudinal POE do not require special analysis, since Fig. 1a shows that the maximum POE values in BTAS and BTGS crystals lie on the X_3 axis: they correspond to the condition $\theta_i = \theta_m = 0°$. For example, by substituting this condition into Eqs. (3) and (7), we can verify that the maximum of the longitudinal POE corresponds to the coefficient π_{33}. It is seen that, for the crystals indicated in Table 2, all maximum values of the IS π'_{ii} (are equal to POC π_{33}) are negative in sign, and prevail by value (–1.48 Br) π'_{ii} for BTGS.

The maximum values of the transverse POE in these crystals and the directions corresponding to these values were determined on the basis of Eqs. (5) and (6) by the method of partial derivatives. Let us determine, for example, the maximum value of the transverse POE in crystals for the case presented in Fig. 1b, and the spherical coordinates of the direction in which it is observed. Based on the surface Eq. (5), let's express its section by the X_2X_3 plane. For this purpose, in (5) let's substitute the condition $\varphi_i = 90°$, which corresponds to such a section:

$$\pi'^{(i)}_{im} = \pi_{12}\sin^2\theta_i + \pi_{31}\cos^2\theta_i + 2\pi_{41}\sin\theta_i\cos\theta_i\,. \tag{11}$$

From the analysis of the partial derivative $\partial\pi'_{im}/\partial\theta_i$, which describes the maximum of the POE π'_{max} in Eq. (11), one obtains an expression for determining the angle θ_i, which characterizes the straight line on which the indicated maximum lies:

$$\theta_i = \frac{1}{2}\mathrm{arctg}\frac{-2\pi_{41}}{\pi_{12} - \pi_{31}} \pm k\pi \;,\; k = 0, 1. \tag{12}$$

For BTAS and BTGS crystals, the angle θ_i is 13° ± 180° and 9° ± 180° respectively (see also Fig. 1b). The maximum POE $\pi'^{(i)}_{im}$ for the indicated values of angle θ_i are observed in the section specified by the already mentioned condition $\varphi_i = 90°$, а также $\varphi_i = 210°$, 330° (for these values of angle φ_i, Eq. (5) is identical to Eq. (11)). It is clear that the indicated angles are related to one another by a rotation of 120°, which corresponds to the third-order symmetry axis $L_3 \parallel X_3(Z)$. By substituting the values of the above angles θ_i into Eq. (11), one obtains the maximum values of the transverse POE: $\pi'^{(i)}_{im} = 1.19$ Br for the BTAS crystal and $\pi'^{(i)}_{im} = 1.33$ Br for BTGS. These POE values are somewhat smaller than for the CTGS crystal and substantially larger than for LGS (see Table 2).

For the other transverse POE $\pi'^{(m)}_{im}$ (the surface is constructed by the radius vector ***R*** **||** ***m***), the maximum values turned out to be much smaller (0.81 and 0.86 Br for BTAS and BTGS crystals, respectively). However, the indicated POE values significantly exceed the maxima of the transverse POE $\pi'^{(m)}_{im}$ in CTGS and LGS crystals (see the last row of Table 2).

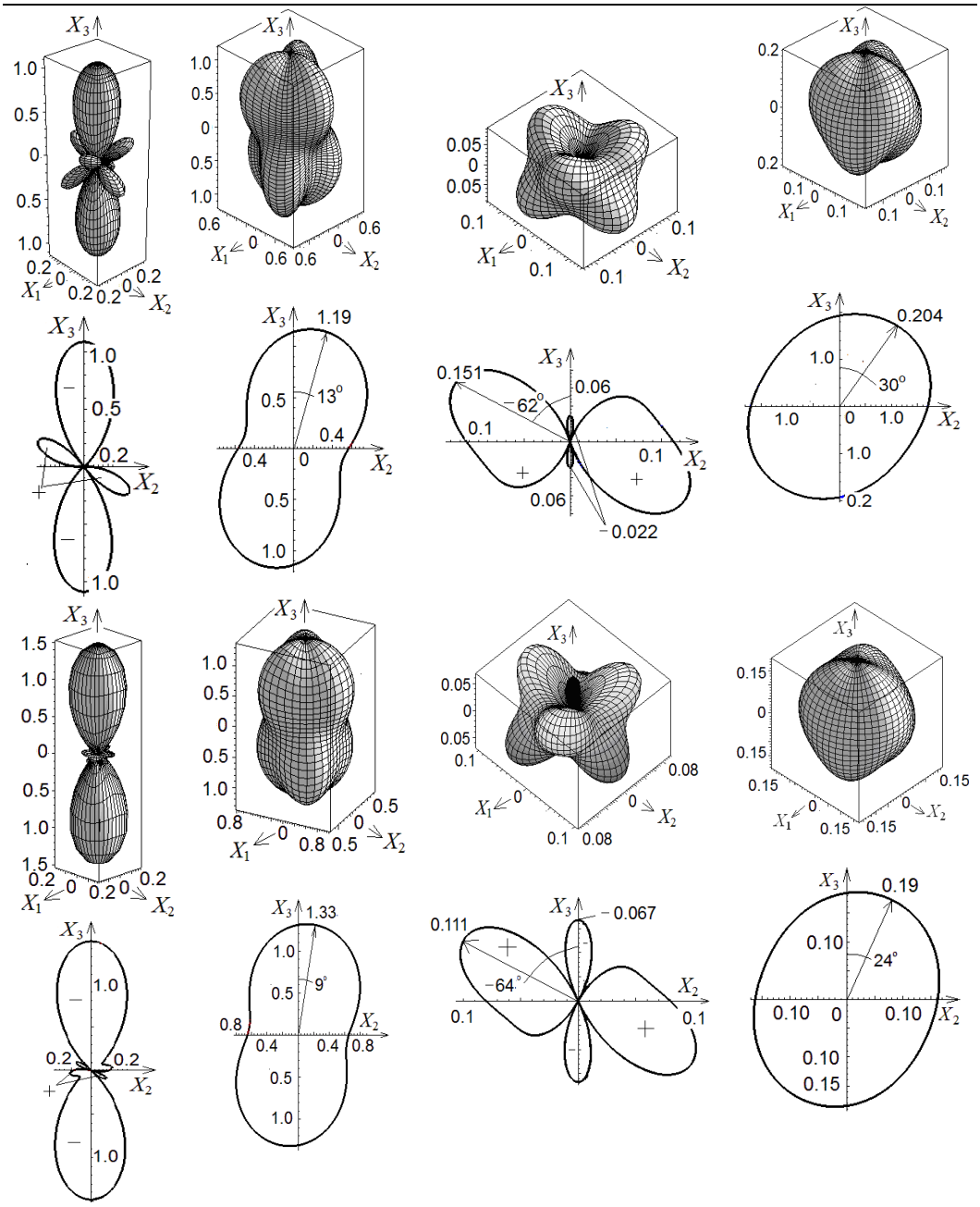

(a) (b) (c) (d)

Fig. 1. Examples of ISs of POE and ELOE and their sections by the X_2X_3 plane for BTAS (top) and BTGS (bottom) crystals: (a) longitudinal POE π'_{ii} (In Br); (b) transverse POE $\pi'^{(i)}_{im}$ (in Br); (c) longitudinal ELOE p'_{ii}; (d) transverse ELOE $p'^{(i)}_{ik}$.

Table 2. Maximum values π'_{max} of ISs of the longitudinal π'_{ii} and transverse $\pi'^{(i)}_{im}$, $\pi'^{(m)}_{im}$ POE, and their angular parameters in BTAS, BTGS, CTGS, and LGS crystals.

IS	BTAS			BTGS			CTGS [25]			LGS [25]		
	π'_{max} Br	$\theta_{i(m)}$, deg	$\varphi_{i(m)}$, deg	π'_{max} Br	$\theta_{i(m)}$, deg	$\varphi_{i(m)}$, deg	π'_{max} Br	$\theta_{i(m)}$, deg	$\varphi_{i(m)}$, deg	π'_{max} Br	$\theta_{i(m)}$, deg	$\varphi_{i(m)}$, deg
π'_{ii}	−1.09	0	0	**−1.48**	0	0	−1.20	0	0	−1.25	0	0
$\pi'^{(i)}_{im}$	1.19	13	90, 210, 330	1.33	9	90, 210, 330	**1.48**	14	90, 210, 330	0.85	24	90, 210, 330
$\pi'^{(m)}_{im}$	0.81	27	90, 210, 330	0.86	32	90, 210, 330	0.77	33	90, 210, 330	0.38	29	90, 210, 330

***Note*:** in the $\theta_{i(m)}$ and $\varphi_{i(m)}$ columns, the indices *i* or *m* refer to the radius $\boldsymbol{R} \parallel \boldsymbol{i}$, which describes the IS of light polarization (the upper index at the $\pi'^{(i)}_{im}$), or the radius vector $\boldsymbol{R} \parallel \boldsymbol{m}$, which describes the IS of mechanical stress (the upper index at the $\pi'^{(m)}_{im}$); in the case of IS π'_{ii} index *i* is equal to index *m*.

By analogy with the POE, the maximum values of the ELOE ISs and the corresponding values of angles θ and φ (see Table 3). Examples of ELOE surfaces for BTAS and BTGS crystals are presented in Fig. 1c,d.

Table 3. Maximum values p'_{max} of ISs of the longitudinal p'_{ii} and transverse $p'^{(i)}_{ik}$, $p'^{(k)}_{ik}$ ELOE, and their angular parameters in BTAS, BTGS, CTGS, and LGS crystals.

IS	BTAS			BTGS			CTGS [25]			LGS [25]		
	p'_{max}	$\theta_{i(k)}$, deg	$\varphi_{i(k)}$, deg	p'_{max}	$\theta_{i(k)}$, deg	$\varphi_{i(k)}$, deg	p'_{max}	$\theta_{i(k)}$, deg	$\varphi_{i(k)}$, deg	p'_{max}	$\theta_{i(k)}$, deg	$\varphi_{i(k)}$, deg
p'_{ii}	0.151	−62	90, 210, 330	0.111	−64	90, 210, 330	−0.088	0	0	−0.181	0	0
$p'^{(i)}_{ik}$	0.204	30	90, 210, 330	0.191	24	90, 210, 330	0.172	13	90, 210, 330	0.094	26	90, 210, 330
$p'^{(k)}_{ik}$	**0.213**	27	90, 210, 330	**0.209**	33	90, 210, 330	0.109	24	90, 210, 330	0.075	15	90, 210, 330

***Note*:** in the $\theta_{i(k)}$ and $\varphi_{i(k)}$ columns, the indices *i* or *k* refer to the radius vector $\boldsymbol{R} \parallel \boldsymbol{i}$, which describes the IS of light polarization (the upper index at the $p'^{(i)}_{ik}$), or the radius vector $\boldsymbol{R} \parallel \boldsymbol{k}$, which describes the IS of strain (the upper index at the $p'^{(k)}_{ik}$); in the case of IS p'_{ii} index *i* is equal to index *k*.

It follows from Table 3 that, in contrast to the POE, the maximum values of both the longitudinal ELOE p'_{ii}, and the two transverse ELOEs $p'^{(i)}_{ik}$ and $p'^{(k)}_{ik}$ of BTAS crystals exceed the corresponding maxima of BTGS crystals. In addition, the maxima of both transverse ELOEs of BTAS and BTGS crystals substantially exceed the corresponding maxima of CTGS and LGS (for example, for the maxima of the surface $p'^{(k)}_{ik}$, this advantage is very large, by a factor of 2-3). Only for the maximum of the longitudinal ELOE (p'_{ii} = −0.181), the LGS crystal has a significant advantage over the other crystals studied.

Let's characterize below the ISs of the ELOE under the action of shear strains. These surfaces are described by Eq. (10) and shown in Fig. 2. This figure also presents examples of sections of the ELOE surfaces in BTAS, BTGS, CTGS, and LGS crystals, on which the maximum ELOE p'_{ik} and the corresponding directions (angles θ_i), along which they are observed, are indicated. These characteristics were found analytically. Namely, the section of surface (10) by the X_2X_3 plane corresponds to the condition $\varphi_i = 90°$, substituting it into (10), one obtains:

$$\begin{aligned} p'_{ik} &= p'(\theta_i, 90°, 45°, 0°) \\ &= 0.5[(p_{12} - p_{13})\sin^2\theta_i + (p_{31} - p_{33})\cos^2\theta_i + p_{41}\sin 2\theta_i]. \end{aligned} \tag{13}$$

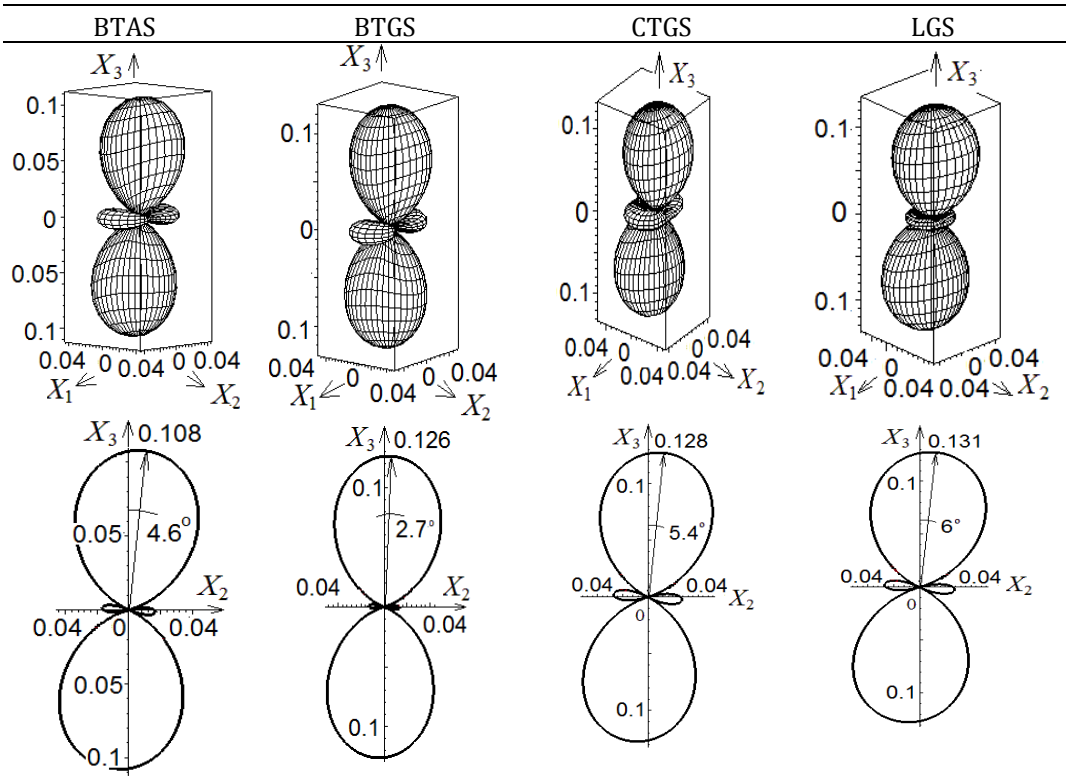

Fig. 2. Examples of ELOE p'_{ik} surfaces (under the action of shear strains) with large effect values and sections of these surfaces by the X_2X_3 plane in the studied crystals.

From the analysis of the partial derivative $\partial p'_{ik} / \partial \theta_i = 0$, one obtains an expression for determining the angle θ_i:

$$\theta_i = \frac{1}{2}\text{arctg}\frac{-2p_{41}}{p_{12} - p_{13} - p_{31} + p_{33}} \pm k\pi, \quad k = 0, 1. \tag{14}$$

By substituting the corresponding ELOC values p_{ik} (Table 1) into (14), one determines the angles θ_i for the indicated crystals. Based on these angles θ_i and expression (13), one obtains the values of the ELOE p'_{ik} maxima under the action of shear strains.

From Fig. 2, it is seen that the ELOE p'_{ik} surfaces induced by shear strains in BTAS, BTGS, CTGS, and LGS crystals demonstrate substantial anisotropy of the effect, while the maximum ELOE values are observed in directions that do not coincide with the crystallophysical axes.

The angle θ_i of the largest ELOE value is small for all crystals, 2.7–6.0°. The maximum values of the surfaces p'_{ik} are comparable for BTGS, CTGS, and LGS crystals (~0.13), whereas the maximum of the surface for BTAS is substantially smaller (0.108).

It should be emphasized that the ELOE maxima for BTAS and BTGS crystals (0.108 and 0.126, respectively, see Fig. 2) are almost twice as small as in the cases of the transverse ELOE (Table 3). However, these ELOE values under shear strain can have a positive effect on the estimation of the acousto-optic figure of merit M_2. This is because transverse acoustic waves (AWs), which induce shear strains, generally have substantially lower acoustic velocities (v) than longitudinal AWs [11, 41]. Accordingly, the M_2 values will be larger, since it is known [42, 43] that $M_2 \sim 1/v^3$.

5. Conclusions

The photoelastic properties of $Ba_3TaAl_3Si_2O_{14}$ (BTAS) та $Ba_3TaGa_3Si_2O_{14}$ (BTGS) crystals have been studied, based on the calculated components of the POC and ELOC matrices and the indicative surfaces (ISs) of POE and ELOE constructed on their basis. The calculation was performed by a quantum-mechanical method using the Crystal*17* program. For the construction and analysis of ISs of other langasite-group crystals, $La_3Ga_5SiO_{14}$ (LGS) та $Ca_3TaGa_3Si_2O_{14}$ (CTGS) POCs and ELOCs were used, that are determined experimentally by interferometric and polarization-optical methods in [22-24].

Based on the IS analysis, the maximum POE and ELOE values and the directions along which these maxima lie were found. Some features of the obtained results are listed below.

1. The maxima of the longitudinal POE π'_{ii} for all the studied crystals lie on the X_3 axis and, accordingly, their values are equal to the POC π_{33}. The signs of the surface π'_{ii} maxima are negative, and BTGS exceeds the other crystals in magnitude (–1.48 Br). The maxima of the transverse POE of light polarization $\pi'^{(i)}_{im}$ are also large (for example, 1.48 Br for CTGS) and lie along directions that form angles of 9–24° with the X_3 axis. All maxima of the transverse POE of mechanical stress $\pi'^{(i)}_{im}$ are considerably smaller, especially for the LGS crystal (0.38 Br).

2. All POE maxima of BTGS crystals exceed the corresponding POE values of BTAS crystals in magnitude. In contrast, BTAS crystals exceed BTGS in the magnitudes of the maxima of both the longitudinal ELOE p'_{ii}, and the two transverse ELOEs $p'^{(i)}_{ik}$, $p'^{(k)}_{ik}$, reaching the large value of $p'^{(k)}_{ik}$ = 0.213. In addition, the maxima of the transverse ELOEs of BTAS and BTGS crystals substantially exceed the corresponding maxima of CTGS and LGS (for example, for the maxima of the $p'^{(k)}_{ik}$ this advantage is very large, by a factor of 2-3). Only for the maximum of the longitudinal ELOE (p'_{ii} = –0.181) the LGS crystal has a significant advantage over the other crystals studied.

3. The ELOE surfaces p'_{ik} induced by shear strains in BTAS, BTGS, CTGS, and LGS crystals demonstrate substantial anisotropy of the effect, while the maximum ELOE values are observed in directions that do not coincide with the crystallophysical axes. For example, the deviation of such directions from the X_3 axis for the indicated crystals is 2.7-6.0°. The maximum values of the ELOE surfaces p'_{ik} of BTAS and BTGS crystals (0.108 and 0.126, respectively) are almost twice as small as in the cases of transverse ELOE. However, the indicated ELOE values can have a positive effect on the estimation of the acousto-optic figure

of merit M_2. This is because transverse acoustic waves (AWs), which induce shear strains, generally have substantially lower velocities, υ, than longitudinal AWs. Accordingly, the M_2 values will be larger, since it is known that $M_2 \sim 1/\upsilon^3$. For comparable M_2 values, BTAS crystals will have an advantage due to their lower cost, resulting from replacing the expensive element Ga with the cheaper element Al.

Funding and acknowledgement. This work was supported by the National Research Foundation of Ukraine (Project 2025.07/0368) and the HORIZON-MSCA-2021-SE-01 Program, agreement number 101086493.

Conflict of interest. Authors declare no conflict of interest.

Authors contribution. N. Demyanyshyn: conceptualization, calculations. B. Mytsyk: conceptualization, validation, editing. O. Lishchuk: original draft preparation. P. Solomenchuk: visualization, original draft preparation. A. Andrushchak: methodology, review & editing.

References

1. Kohn, W., & Sham, L. (1965). Self-consistent equations including exchange and correlation effects. *Physical Review*, *140*(4A), A1133-A1138.
2. Parr, R.G., & Yang, W. (1989). *Density-functional theory of atoms and molecules*. New York – Oxford, Oxford University Press.
3. Johnson, B.G., Gill, P.M., & Pople J.A. (1993). The performance of a family of density functional methods. *Journal of Chemical Physics*, *98*(7), 5612-5626.
4. Perdew, J., Ruzsinszky, A., Csonka, G., Vydrov, O., Scuseria, G., Constantin, L., Zhou, X., & Burke, K. (2008). Restoring the density-gradient expansion for exchange in solids and surfaces. *Physical Review Letters*, *100*(13), 136406.
5. Konstantinova, A., Golovina, T., Nabatov, B., Dudka, A., & Mill B. (2015). Experimental and theoretical determination of the optical rotation in langasite family crystals. *Crystallography Reports*, *60*(6), 907-914.
6. Amina, Uzair, M., Khan, A.S., Quraishi, A.M., Almahri, A., Soliyeva, M., Tirth, V., Algahtani, A., Abdullah, Mohammed, R.M., Sarker, M.R., Hadia, N.M.A., & Zaman, A. (2024). Study of structural, electronic, optical and mechanical properties of K_2ScCuF_6 and K_2YCuF_6 perovskites via DFT calculations. *Results in Physics*, *62*(**7**), 107845.
7. Rudysh, M., Shchepanskyi, P., Fedorchuk, A., Brik, M., Stadnyk, V., Myronchuk, G., Kotomin, E., & Piasecki, M. (2021). Impact of anionic system modification on the desired properties for $CuGa(S_{1-x}Se_x)_2$ solid solutions. *Computational Materials Science*, *196*(8), 110553.
8. Chung, Ch. Y., Yaokawa, R., Mizuseki, H., & Kawazoe, Y. (2011). Atomistic configurational effects on piezoelectric properties of $La_3Ta_{0.5}Ga_{5.5}O_{14}$ and a new piezoelectric crystal design. *Acta Materialia*, *59*(16), 6473-6479.
9. Mytsyk, B., Kryvyy, T., Demyanyshyn, N., Mys, O., Martynyuk-Lototska, I., Kokhan, O., & Vlokh, R. (2018). Piezo-, elasto- and acousto-optic properties of Tl_3AsS_4 crystals. *Appl. Opt.*, *57*(14), 3796-3801.
10. Mytsyk, B., Andrushchak, A., Vynnyk, D., Demyanyshyn, N., Kost, Y., & Kityk, A. (2020). Characterization of photoelastic materials by combined Mach-Zehnder and conoscopic interferometry: Application to tetragonal lithium tetraborate crystals. *Optics and Lasers in Engineering*, *127*, 105991.
11. Kaminskii, A., Belokoneva, E., Mill, B., Pisarevskii, Yu., Sarkisov, S., Silvestrova, I., Butashin, A., & Khodzhabagyan, G. (1984). Pure and Nd^{3+}–doped $Ca_3Ga_2Ge_4O_{14}$ and $Sr_3Ga_2Ge_40_{14}$ single crystals, their structure, optical, spectral luminescence, electromechanical properties, and stimulated emission. *Physica Status Solidi (a)*, *86*, 345-362.
12. Andreev I. (2004). Two decades following the discovery of thermallys table elastic properties of $La_3Ga_5SiO_{14}$ crystal and coining of the term langasite. *Technical Physics*, *49*(9), 1101-1103.
13. Remark, T., Segonds, P., Debray, J., Jegouso, D., Villora, E.G., Shimamura, K., & Boulanger, B., Linear and nonlinear optical properties of the langasite crystal $Ca_3TaAl_3Si_2O_{14}$. (2023). *Optical Materials Express*, *13*(7), 2053-2060.
14. Kong, H., Wang, J., Zhang, H., Yin, X., Zhang, Sh., Liu, Ya., Cheng, X., Gao, L., Hu, X., & Jiang, M. (2003). Growth, properties and application as an electrooptic Q-switch of langasite crystal. *Journal of Crystal Growth*, *254*(3-4), 360-367.

15. Irzhak, D., & Roshchupkin, D. (2018). Measurement of independent piezoelectric moduli of $Ca_3NbGa_3Si_2O_{14}$, $La_3Ga_{5.5}Ta_{0.5}O_{14}$ and $La_3Ga_5SiO_{14}$ single crystals. *Journal of Applied Crystallography*, *51*, 1174-1181.
16. Chani, V., Shimamura, K., Yu, Y., & Fukuda, T. (1997). Design of new oxide crystals with improved structural stability. *Journal of Materials Science and Engineering*, *R20*, 281-338.
17. Zheng, Y., Cui, S., Chen, J., Tu, X., Xin, J., Kong, H., & Shi, E. (2013). Advances in design, growth and application of piezoelectric crystals with langasite structure. *Proc. Symposium on Piezoelectricity, Acoustic Waves, and Device Applications (SPAWDA), Shanghai, China, 23–25 November 2012; IEEE Xplore: Piscataway, NJ, USA,* 252-259.
18. Fritze, H. (2010). High-temperature bulk acoustic wave sensors. *Measurement Sciense and Technology*, *22*(1), 012002.
19. Xin, Y., Shaojun, Z., & Jiyang, W. (2005). Mutual action of the optical activity and the electro-optic effect and its influence on the $La_3Ga_5SiO_{14}$ crystal electro-optic Q switch. *Journal of the Optical Society of America B*, *22*(2), 394-397.
20. Zhang, J., Tan, Q., Zhang, L., Zhao, N., & Liang, X. (2022). Langasite bonding via high temperature for fabricating sealed microcavity of pressure sensors. *Micromachines*, *13*(3), 479.
21. Kong, H., Wang, J., Zhang, H., Yin, X., Zhang, Sh., Liu, Ya., Cheng, X., Gao, L., Hu, X., & Jiang, M. (2003). Growth, properties and application as an electrooptic Q-switch of langasite crystal. *Journal of Crystal Growth*, *254*(3-4), 360-367.
22. Mytsyk, B., Andrushchak, A., & Gaskevich, G. (2007). Comprehensive studies of piezo-optical effect in langasite crystals. *Ukrainian Journal of Physics*, *52*(8), 798-808.
23. Mytsyk, B., Demyanyshyn, N., Andrushchak, A., Kost', Y., Parasyuk, O., & Kityk A. (2010). Piezooptical coefficients of $La_3Ga_5SiO_{14}$ and $CaWO_4$ crystals: A combined optical interferometry and polarization-optical study. *Optical Materials*, *33*(1), 26-30.
24. Mytsyk, B., Suhak, Yu., Demyanyshyn, N., Buryy, O., Syvorotka, N., Sugak, D., Ubizskii, S., & Fritze, H. (2020). Full set of piezo-optic and elasto-optic coefficients of $Ca_3TaGa_3Si_2O_{14}$ crystals at room temperature. *Applied Optics*, 59(28), 8951-8958.
25. Demyanyshyn, N., Suhak, Yu., Mytsyk, B., Buryy, O., Maksishko, Yu., Sugak, D., & Fritze, H. (2021). Anisotropy of piezo-optic and elasto-optic effects in langasite family crystals. *Optical Materials*, *119*(9), 111284.
26. Mys, O., Kostyrko, M., & Vlokh R. (2025). Anisotropy of acousto-optic figure of merit in Tl_3AsS_4 crystals. anisotropic diffraction. *Ukrainian Journal of Physical Optics*, *26*(2), 02080-02088.
27. Mys, O., Kostyrko, M., & Vlokh, R. (2025). Effect of magnetic field on the efficiency of isotropic acousto-optic diffraction in optically resistant β-BaB_2O_4 crystals. *Ukrainian Journal of Physical Optics*, *26*(1), 01023-01031.
28. Mys, O., Kostyrko, M., Krupych, O., & Vlokh, R. (2015). Anisotropy of the acoustooptic figure of merit for $LiNbO_3$ crystals. Isotropic diffraction. *Applied Optics*, *54*(27), 8176-8186.
29. Buryy, O. A., Andrushchak, A. S., Kushnir, O. S., Ubizskii, S. B., Vynnyk, D. M.,.Yurkevych, O. V., Larchenko, A. V., Chaban, K. O., Gotra, O. Z., & Kityk, A. V. (2013). Method of extreme surfaces for optimizing geometry of acousto-optic interactions in crystalline materials: Example of $LiNbO_3$ crystals. *Journal of Applied Physics*, *113*(8), 083103.
30. Demyanyshyn, N.M., Mytsyk, B.G., Kost, Y.P., Solskii, I.M., & Sakharuk, O.M. (2015). Elasto-optic effect anisotropy in calcium tungstate crystals. *Applied Optics*, *54*(9), 2347-2355.
31. Mytsyk, B., Erba, A., Maul, J., Demyanyshyn, N., Shchepanskyi, P., & Syrotynsky, O. (2023). Photoelasticity of CNGS crystals. *Applied Optics*, *62*(30), 7952-7959.
32. Buryy, O., Demyanyshyn, N., Mytsyk, B., Andrushchak, A. (2016). Optimizing of the piezo-optic interaction geometry in SrB_4O_7 crystals. *Optica Applicata*, *46*(3), 447-459.
33. Usui, H., Kusakabe, H., Tokuda, M., Sugiyama, K., Hoshina, T., Tsurumi, T., & Takeda, H. (2020). Structure and electrical properties of $Ba_3TaGa_3Si_2O_{14}$ single crystals grown by Czochralski method. *Journal Ceramic Society of Japan*, *128*(8), 441-446.
34. Demyanyshyn, N., Buryy, O., Mytsyk, B., Solomenchuk, P., Lishchuk, O., & Andrushchak, A. (2025). Spatial anisotropy of photoelasticity determined by path difference in $Ba_3TaGa_3Si_2O_{14}$ cystals. *Crystals*, *15*(8), 708.
35. Erba, A., Ruggiero, M.T., Korter, T.M., & Dovesi, R. (2015). Piezo-optic tensor of crystals from quantum-mechanical calculations. *The Journal of Chemical Physics*, *143*(14), 144504.
36. Mytsyk, B., Erba, A., Demyanyshyn, N., & Sakharuk, O. (2016). Piezo-optic and elasto-optic effects in lead molibdate crystals. *Optical Materials*, *62*(32), 632-638.
37. Erba, A., & Dovesi, R. (2013). Photoelasticity of crystals from theoretical simulations. *Physical Review B*, *88*(4), 045121.
38. Chung, Ch. Y., Yaokawa, R., Mizuseki, H., & Kawazoe, Y. (2012). Tantalum vacancy effects on electrical Conductivityof $La_3Ta_{0.5}Ga_{5.5}O_{14}$ без and Ba-based P321 Crystals. *Key Engineering Materials*, *508*, 325-330.

39. Nye, J.F. (1964). *Physical properties of crystals*. Oxford, Oxford Clarendon Press.
40. Narasimhamurty, T.S. (1981). *Photoelastic and electro-optic properties of crystals*. New York – London, Plenum Press.
41. Buryy, O., Demyanyshyn, N., Mytsyk, B., Andrushchak, A., & Sugak, D. (2022). Acousto-optic interaction in LGS and CTGS crystals. *Optics Continuum*, *1*(6), 1314-1323.
42. Dixon, R.W. (1967). Photoelastic properties of selected materials and their relevance for applications to acoustic light modulators and scanners. *Journal of. Applied Physics*, *38*(13), 5149-5153.
43. Uchida, N., & Niizeki, N. (1973). Acoustooptic deflection materials and techniques. Proceedings of the IEEE, *61*(8), 1073-1092.

Demyanyshyn, N., Mytsyk, B., Lishchuk, O., Solomenchuk, P., Andrushchak, A. (2026). Extreme Values of Photoelastic Effects in BTAS and BTGS Crystals**.** *Ukrainian Journal of Physical Optics*, *27*(2), 02157 – 02168. doi: 10.3116/16091833/Ukr.J.Phys.Opt.2026.02157

Анотація. *Вказівні поверхні (ВП) просторового розподілу п'єзооптичнного та пружнооптичного ефектів (ПОЕ та ПрОЕ) у кристалах типу лангаситу $Ba_3TaAl_3Si_2O_{14}$ (BTAS) та $Ba_3TaGa_3Si_2O_{14}$ (BTGS) були побудовані на основі матриць п'єзооптичних π_{im} та пружнооптичних p_{in} коефіцієнтів, отриманих із розрахунків з перших принципів. Ми представили співвідношення для ВП поздовжнього та поперечного ПОЕ та ПрОЕ, а також співвідношення для ПрОЕ, індукованого деформаціями зсуву. Показано, що властивості ПОЕ та ПрОЕ кристалів BTAS та BTGS є суттєво анізотропними, а найбільші значення поперечного ПрОЕ кристалів BTAS та BTGS (0,213 та 0,209 відповідно) не збігаються з напрямками кристалофізичних осей цих кристалів. Згідно із вказаними значеннями ПрОЕ ці кристали переважають інші кристали групи лангаситу, $La_3Ga_5SiO_{14}$ (LGS) та $Ca_3TaGa_3Si_2O_{14}$ (CTGS), у 2-3 рази. Для всіх вищезазначених кристалів були побудовані поверхні ПрОЕ, індуковані зсувними деформаціями. Максимальні значення цих поверхонь (0,108-0,131) практично вдвічі поступаються максимумам поперечного ПрОЕ кристалів BTAS та BTGS, але акустооптична ефективність може бути відносно високою завдяки низьким швидкостям акустичних хвиль, які зумовлені зсувними деформаціями.*

Ключові слова: *фотопружність, квантово-механічний розрахунок, кристали групи лангаситу, вказівні поверхні*